1-1-2000

Applications of magnetic resonance in model systems: Cancer therapeutics

Jeffrey L. Evelhoch
Wayne State University

Robert J. Gillies
University of Arizona Cancer Center

Gregory S. Karczmar
The University of Chicago

Jason A. Koutcher
Memorial Sloan-Kettering Cancer Center

Ross J. Maxwell
Cancer Research UK

See next page for additional authors

Neoplasia • Vol. 2, Nos. 1–2, January-April 2000, pp. 152–165 152

www.nature.com/neo

Applications of Magnetic Resonance in Model Systems: Cancer Therapeutics[1]

Jeffrey L. Evelhoch, Robert J. Gillies†, Gregory S. Karczmar‡, Jason A. Koutcher§, Ross J. Maxwell¶, Orhan Nalcioglu#, Natarajan Raghunand†, Sabrina M. Ronen**, Brian D. Ross†† and Harold M. Swartz ‡‡*

*Cancer Biology Program, Barbara Ann Karmanos Cancer Institute and Departments of Internal Medicine and Radiology, Wayne State University, Detroit, MI; †Department of Biochemistry, Arizona Cancer Center, Tucson, AZ; ‡Department of Radiology, University of Chicago, Chicago, IL; §Department of Medical Physics, Memorial Sloan-Kettering Cancer Center, New York, NY; ¶Gray Laboratory Cancer Research Trust, Northwood, Middlesex, UK; #Health Sciences Research Imaging Center, College of Medicine, University of California, Irvine, CA; **CRC Clinical Magnetic Resonance Research Group, Institute of Cancer Research, Royal Marsden Hospital, Downs Road, Sutton Surrey, UK; ††Department of Radiology and Biological Chemistry, University of Michigan Medical School, Ann Arbor, MI and ‡‡EPR Center for the Study of Viable Systems, Dartmouth Medical School, Hanover, NH

Abstract

The lack of information regarding the metabolism and pathophysiology of individual tumors limits, in part, both the development of new anti-cancer therapies and the optimal implementation of currently available treatments. Magnetic resonance [MR, including magnetic resonance imaging (MRI), magnetic resonance spectroscopy (MRS), and electron paramagnetic resonance (EPR)] provides a powerful tool to assess many aspects of tumor metabolism and pathophysiology. Moreover, since this information can be obtained non-destructively, pre-clinical results from cellular or animal models are often easily translated into the clinic. This review presents selected examples of how MR has been used to identify metabolic changes associated with apoptosis, detect therapeutic response prior to a change in tumor volume, optimize the combination of metabolic inhibitors with chemotherapy and/or radiation, characterize and exploit the influence of tumor pH on the effectiveness of chemotherapy, characterize tumor reoxygenation and the effects of modifiers of tumor oxygenation in individual tumors, image transgene expression and assess the efficacy of gene therapy. These examples provide an overview of several of the areas in which cellular and animal model studies using MR have contributed to our understanding of the effects of treatment on tumor metabolism and pathophysiology and the importance of tumor metabolism and pathophysiology as determinants of therapeutic response. *Neoplasia* (2000) **2,** 152–165.

Keywords: nuclear magnetic resonance, neoplasms, pathophysiology, metabolism, therapy.

Introduction

The development of new anti-cancer therapies and the optimal implementation of currently available treatments are limited, in part, by the lack of information regarding the metabolism and pathophysiology of individual tumors. Availability of this metabolic and physiologic information for individual tumors could be used in a variety of ways including the following 1) It could guide the development of new strategies to manipulate tumor physiology and/or metabolism for therapeutic advantage, 2) It could allow the effects of treatment on tumor pathophysiology to be considered in scheduling multi-course or multi-modality treatment, 3) It may allow use of changes in tumor pathophysiology evident, prior to changes in tumor size, to detect tumor response to therapy in individual patients early in the course of treatment. One promising method to non-invasively assess tumor physiology and metabolism, which can be applied to cell and animal models and is also already widely available clinically, is magnetic resonance (MR).

Magnetic resonance imaging (MRI), magnetic resonance spectroscopy (MRS), and electron paramagnetic resonance (EPR) can non-invasively provide a wealth of information regarding tumor metabolism and pathophysiology. Moreover, because MR provides information regarding *in vivo* tumor metabolism and pathophysiology non-destructively, pre-clinical results from cellular or animal models are often easily translated into the clinic. This review presents selected applications to give the reader an overview of several of the areas in which cellular and animal model studies using MR have contributed to our understanding of the effects of treatment on tumor metabolism and pathophysiology and the importance of tumor metabolism and pathophysiology as determinants of therapeutic response. A companion review [1] focuses on the use of MR to investigate tumor biology and physiology in the absence of treatment.

Address all correspondence to: Dr. Jeffrey L. Evelhoch, Harper Hospital MR Center, 3990 John R. Street, Detroit, MI 48201. E-mail: evelhoch@med.wayne.edu

[1]USPHS grant CA43113 (J.L.E.); USPHS grant CA83041 and the Flinn Foundation (R.J.G.); USPHS grant CA75476 (G.S.K.); DAMD17-98-1-8153 (J.A.K.); UC Biotechnology Program grant 97-08 and California BCRP grant 3IB-0028 (O.N.); USPHS grant CA77575 (N.R.); UKCRC grant SP1780/0103 (S.M.R.); USPHS grants GM51630 and RR11602 (H.M.S.).

Received 29 November 1999; Accepted 13 December 1999.

MR and Apoptosis

Apoptosis, or programmed cell death, is a physiological, genetically controlled and morphologically defined process of cell suicide. It is required for the normal development of multicellular organisms, essential, for example, in embryonic morphogenesis or lymphocyte selection. First described on the basis of morphological observations [2], the precise mechanism and genetic regulation of apoptosis are still under investigation (Ref. [3] and references therein). In the context of cancer, however, it is now clear that cell death following chemotherapeutic treatment will occur, in most cases, by apoptosis [4]. Conversely, resistance to chemotherapy can be affected by the expression of genes regulating the apoptotic pathway. Non-invasively identifying MR signals that are correlated with programmed cell death could therefore be useful both in contributing to the understanding of apoptosis and in helping assess tumor response *in vivo*. To date, however, most MR studies of apoptosis have investigated *in vitro* cell systems.

Membrane Changes Associated with Apoptosis

End-stage apoptosis is characterized by cell shrinkage, blebbing and shedding of apoptotic bodies, as well as alterations in the distribution of phospholipids within the plasma membrane. Cell shrinkage can be monitored by using diffusion-weighted ^{1}H MRS to assess changes in intracellular volume [5,6]. Other ^{1}H MRS studies have also identified increases in cellular fatty acid signals (resonating at 1.3, 2.8 and 5.4 ppm). These have been attributed either to a decrease in membrane microviscosity during apoptosis or to an increase in intracellular triglycerides and free fatty acids following activation of phospholipase A2 during cell death [7,8]. Further changes in cellular lipid metabolism during apoptosis have been identified using ^{31}P MRS. A significant drop in phosphocholine (PCho) has been observed in several different cell lines following apoptosis induced by various chemotherapeutic treatments [8–13]. In HL-60 cells, the drop in PCho was also accompanied by an accumulation of CDP-choline and an inhibition of the CDP-choline: 1,2-DAG cholinephosphotransferase, possibly due to cellular acidification during apoptosis [10]. No accumulation of CDP-choline was observed in other cell lines. In MCF-7 cells, the drop in PCho was due to inhibition in choline uptake followed by an increase in activity of the CTP:PCho cytidyltransferase [14]. In contrast to these observations, an increase in PCho signal was observed in TNF-induced apoptosis in neutrophils [15]. PCho could be generated as the by-product of sphingomyelin breakdown to produce ceramide — a possible second messenger in TNF as well as fas-induced apoptosis. However, in fas-induced apoptosis of Jurkat cells, no increase in PCho content or drop in sphingomyelin could be observed [9], further contributing to the current controversy regarding the involvement of ceramide in apoptotic signaling.

Energetic Changes Associated with Apoptosis

Apoptosis is an energy-requiring process. At the same time, it is now clear that cytochrome *C* release from the mitochondria is an important step in the apoptotic cascade, possibly diminishing the cell's ability to generate ATP. How cellular ATP stores evolve during apoptosis is therefore an interesting question and ^{31}P MRS could be useful in providing an answer. Some researchers have observed an initial transient increase in cellular nucleoside triphosphates (NTP, predominantly ATP) content during apoptosis [16,17] possibly explained by upregulation of bcl2 in some cell lines following treatment. In contrast to these results, several studies have observed a steady decrease in cellular ATP following induction of cell death (Refs. [9,11–13]; see Figure 1). This drop in ATP has been correlated in most cases with a reduction in cellular NAD/H, and it remains unclear whether ATP is primarily consumed by the cell to replenish its NAD/H stores or whether the drop in high-energy phosphates reflects their utilization in apoptosis. Finally, in several cell systems, the drop in NAD/H content during apoptosis was accompanied by an accumulation of glycolytic intermediates, in particular fructose-1,6-bisphosphate (see Figure 1; Refs. [9,12,13]). This is due to activation of the enzyme poly(ADP-ribose) polymerase

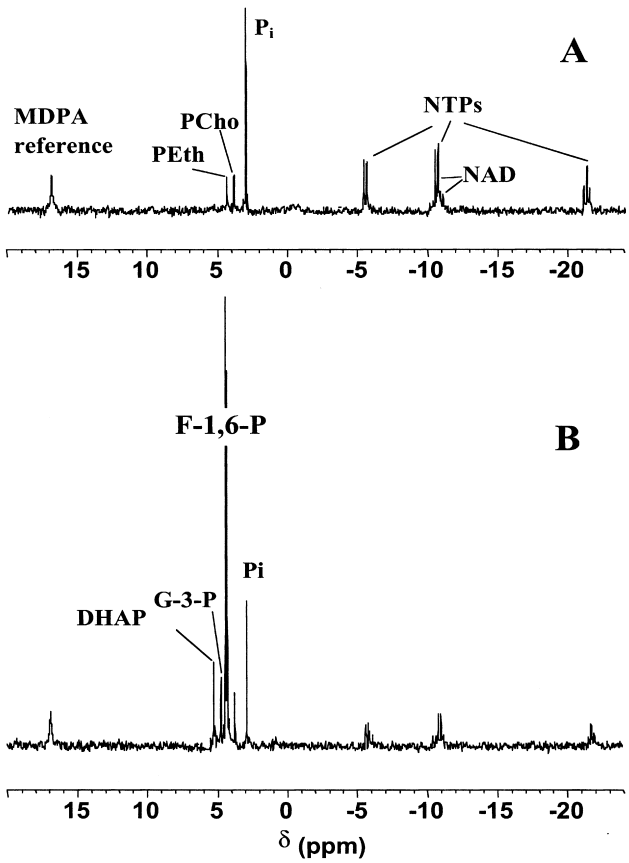

Figure 1. *^{1}H-decoupled ^{31}P MR spectra of extracts from (A) control L1210 cells and (B) apoptosing L1210 cells following 3 hours of treatment with 50 μM nitrogen mustard. Spectra were acquired on a 250-MHz Bruker spectrometer and are the result of 10,000 fully relaxed scans plotted with a line broadening of 0.5 Hz. F-1, 6-P: fructose-1, 6-bisphosphate; G-3-P: glycerol-3-phosphate; DHAP: dihydroxyacetone phosphate.*

(PARP) following chemotherapy-induced DNA damage. Activated PARP consumes NAD, the depletion of which leads to inhibition of the glycolytic enzyme glyceraldehyde-3-phosphate dehydrogenase leading to the accumulation of fructose-1,6-bisphosphate as well as other intermediates.

In spite of some promising *in vivo* results [8], the usefulness of MR techniques in identifying apoptosis in patients still needs to be confirmed. *In vivo*, not only is the spectral resolution lower, but apoptosing cells are rapidly phagocytosed. In most cases, only a small proportion of apoptotic cells is present at any one time (e.g., see Ref. [18]). The spectra recorded from a treated tumor would therefore include a relatively small contribution from the apoptotic fraction. Nonetheless, MR techniques can clearly be useful both in monitoring changes such as cell shrinkage, already known to occur during apoptosis, and in identifying metabolic changes that had not been previously reported.

Early Detection of Therapeutic Response

Traditional methods for detection of therapeutic response generally rely on a gross decrease in tumor size (often measured radiographically using two orthogonal dimensions). Although these methods are useful for assessing response at the end of treatment, little information is available early in the course of treatment (i.e., success or failure of therapy generally takes 2 to 4 months to become apparent). Consequently, patients with non-responsive tumors receive a full-course of toxic therapy without benefit. Hence, the need for early predictors of tumor responsiveness applicable to commonly used therapeutic modalities has long been recognized. Such a predictor would not only allow patients with non-responsive tumors to avoid the side effects and toxicity of a full-course of therapy, they could aid in the selection and evaluation of patients participating in clinical trials of new anti-tumor therapies.

One approach being evaluated as an early-response predictor is to assess tumors before and during treatment in an attempt to detect changes in the pathophysiology of tumors responding to the initial therapy. Because of the ability of MR to non-invasively evaluate tumor metabolism and physiology [1], several MR-based methods have been evaluated for their ability to detect treatment-induced changes occurring within the tumor prior to a decrease in tumor size. Ideally, one would like to be able to detect such changes at the highest possible spatial resolution to permit intra-tumor heterogeneity to be assessed. This section reviews two imaging-based methods with sufficient spatial resolution to assess macroscopic heterogeneity, measurement of water diffusion and dynamic contrast-enhanced MRI (DCE-MRI), which probe different aspects of tumor pathophysiology.

Diffusion MR

Water self-diffusion measured by pulsed-field gradient MR [19] is influenced by the restriction of diffusion due to the limited permeability of cell membranes to water [20]. Hence, the water self-diffusion coefficient measured by MR is referred to as the apparent diffusion coefficient (ADC) and is sensitive to biophysical characteristics of tissue, including the fraction of water in the extracellular space [21]. Commonly used anti-cancer agents are cytotoxic, resulting in tumor cells shrinking (apoptosis) or rupturing (necrosis) — both processes that should increase the extracellular water fraction. Since both radiation [22] and chemotherapy [23] have been shown to substantially increase the fraction of extracellular water, tumor water ADC should be altered by treatment. If these changes are evident prior to a decrease in tumor size, diffusion MRI could provide a clinically applicable response predictor since diffusion MRI has been applied to human brain tumors [24,25], breast [26], liver [27], pancreas [28], and kidney [29].

Treatment response studies thus far have employed rodent tumor models. A dose-dependent, reversible increase in tumor water ADC was observed in RIF-1 tumors (a murine fibrosarcoma) within 2 days of treatment with cyclophosphamide [30]. Even in these RIF-1 tumors treated with doses of cyclophosphamide producing an estimated tumor cell kill of 67%, tumor water ADC increases substantially at a time when there is essentially no change in tumor volume. In rat intracranial 9L gliomas treated with a dose of BCNU resulting in an estimated 90% cell kill, tumor water ADC increased substantially within a week of treatment, while the tumor volume doubled over that time [31]. Ganciclovir treatment of BT4C rat gliomas sensitized by thymidine kinase-mediated gene therapy (see Gene Therapy section) increased tumor water ADC within 4 days after treatment, although tumor growth continued over that period [32,33]. Taxol treatment of MCF-7/s (taxol-sensitive) and MCF-7/d40 (taxol-resistant) human breast cancer xenografts growing in mice increased tumor water ADC only in the drug-sensitive MCF-7/s tumors [34]. For chemically induced rat mammary tumors treated with 100 mg kg^{-1} 5-fluorouracil (5-FU), although all tumors decreased significantly in volume over the first 7 days after treatment, tumors with a high initial ADC started to regrow after 7 days [35]. Collectively, these results provide strong support for the potential of tumor water ADC measurements to provide a sensitive early indicator of response to cytotoxic therapy.

Since each patient's tumor is unique, for ADC measurements to be clinically useful as an early response indicator, the relationship between drug efficacy and the change in ADC (the effective "dose–response" relationship) should not depend on the tumor. Because experimental conditions that can alter the dependence of ADC on the tumor biophysical characteristics vary among laboratories, it is difficult to compare results between laboratories. Consequently, the effects of 5-FU on tumor water ADC measured using the same experimental parameters were examined in three different murine tumors [RIF-1 and two colon adenocarcinomas, Colon-26 and Colon-38 [36]]. A comparison of the therapeutic response [assessed by the specific tumor growth delay, STGD [37]] and corresponding maximum ADC changes indicates a strong "dose–response" relationship for all three tumors (see Figure 2). Considering the RIF-1 cyclophosphamide data with these

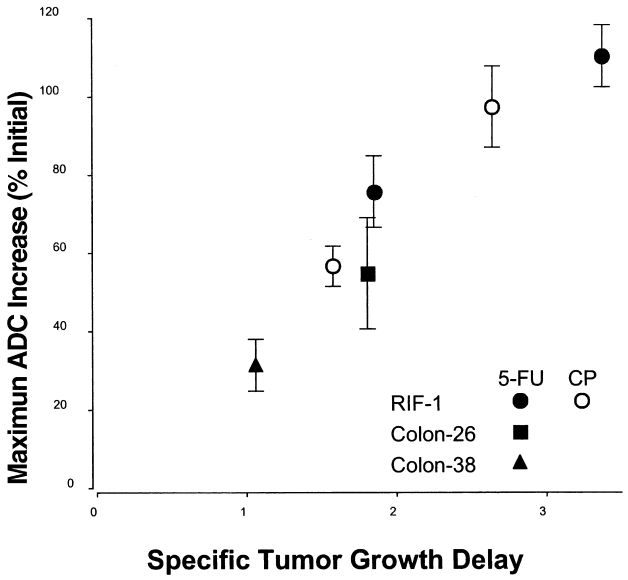

Figure 2. *Relationship between the "dose", as indicated by the therapeutic effect (or STGD), and the "response", as indicated by the maximum increase in tumor water ADC for two chemotherapeutic agents (cyclophosphamide and 5-FU) and three tumor lines (RIF-1, Colon-26 and Colon-38).*

results, it appears the relationship between the maximum change in ADC and therapeutic effect may be independent of the cytotoxic agent, as well as the tumor. These observations support the hypothesis that changes in ADC induced by cytotoxic therapy are associated with changes in tumor pathophysiology due to cell death and are directly related to a therapeutic response. Hence, MR measurements of tumor water ADC for early detection of response to cytotoxic therapy should be generally applicable.

DCE-MRI

As described in the companion article [1], information on several aspects of tumor vascularity (e.g., blood volume, perfusion, permeability) can be derived from analysis of the intra-tumor kinetics of MR contrast agents obtained using DCE-MRI. Since this technique is non-invasive, the tumor can be monitored longitudinally over a period of time to study the changes in tumor vascularity occurring during growth and alterations induced by various kinds of therapy. Initial results in the clinic using the low molecular weight agent, Gd-DTPA, indicate that DCE-MRI may be valuable for both diagnosis [38,39] and prognosis [40,41] of cancer. While these results suggest that there are substantial physiologic differences (i.e., between benign and malignant, or between non-responsive and responsive tumors), the clinically approved low molecular weight agent does not distinguish between changes in perfusion and permeability. Hence, larger molecular weight contrast agents, which can provide an independent measure of vascular permeability, may provide additional critical information. Since they are not yet clinically approved, the ability of these large molecular weight contrast agents to provide an early indication of treatment response has been studied in rodent tumor models.

DCE-MRI with large molecular weight contrast agents indicates changes in tumor vascularity early after treatment for several treatment modalities. In R3230 mammary adenocarcinomas, vascular permeability to albumin-Gd-DTPA is elevated significantly in irradiated tumors compared to control non-irradiated tumors [42,43]. In these same tumors, the vascular volume measured by a macromolecular agent gadomer-17 (molecular weight ~35 kDa) stays constant over 2 weeks in control tumors despite its rapid growth [44]. After treatment with a combination of mitomycin-C and flavone acetic acid, the mean vascular volume decreased by 42% in responders after a week and further down to 56% in week 2 [44].

In another study, DCE-MRI was used to examine the effects of using cytokine therapy to modulate the allogenic rejection of C6 glioma cells implanted subcutaneously into Wistar rats (see Table 1). Adenoviruses expressing mouse interleukin 1-α (IL1-α), mouse interferon γ (IFN-γ), and human transforming growth factor β (TGF-β) were intratumorally injected into three rats, one from each kind. Although the tumor size in both control and rIL-1α-infected animals increased at day 4 (+72% and +140%, respectively), the vascular volume of control tumors decreased by 62% (compared to baseline), while the rIL-1α-inoculated animal had an increase of 41%. These changes of vascular volume at day 4 were predictive of tumor growth several days later. At day 7, the size of control tumors had decreased by 40% while that of the rIL-1α-infected tumors increased by 159%. The predictive value was valid for both unmodulated allogenic tumor rejection and when there was modulation of an immune response (the rIL1-α-treated animal), resulting in a delayed onset of tumor rejection. Immune modulation that increased the immune response (rTGF-β and rIFN-γ) resulted in an accelerated tumor rejection which prevented the evaluation of vascular volume as a predictive tool. These studies support the use of DCE-MRI as a practical tool in the assessment of tumor vascularity to evaluate therapeutic response. As macromolecular contrast agents become more widely available for clinical use, non-invasive evaluation of changes in vascular volume following cancer therapy can be performed.

Biochemical Modulators of Therapeutic Response

Cell kill for most commonly used chemotherapeutic agents is thought to occur by damage to DNA [45]; historically, most chemotherapeutic agents have focused on inhibition or poor

Table 1. The Percentage Change in Tumor Size and the Volume (V_b) in Control and Gene-Therapy-Treated Tumors.

Group	Percent Change in Tumor Volume		Percent Change (V_b)
	Day 4/Day 0	Day 7/Day 4	Day 4/Day 0
Control	+72	−40	−62
IL1-α	+140	+159	+41
TGF-β	−80	−83	NA
IFN-γ	−94	−100	NA

fidelity of DNA reproduction. Recent studies have suggested that other targets for anti-tumor agents, such as the tumor vasculature, microtubular structure, cell membrane, intracellular milieu, pH, or metabolic pathways, could enhance tumor destruction or inhibit proliferation. A novel approach to treating tumors is to use traditional chemotherapeutic agents in combination with drugs aimed at interfering with tumor metabolism, i.e., agents that inhibit glycolysis, aerobic metabolism, etc. These agents often have limited, if any, activity by themselves, but can potentiate the effect of other drugs or radiation. Examples of these agents include 2-deoxyglucose (2-DG), lonidamine (LON), and 6-aminonicotinamide (6-AN).

6-Aminonicotinamide

6-AN, an analogue of niacin, is currently being evaluated in pre-clinical trials as part of a combination chemotherapy and as a radiosensitizer [46–49]. Although 6-AN was evaluated in clinical trials about 40 years ago and lacked efficacy [50], *in vitro* studies have shown 6-AN to sensitize cells to radiation [51] *cis*-platinum [52] and 1,3 Bis(2-chloroethyl)-1-nitrosourea (BCNU) [53]. 6-AN acts by competition with niacin in pathways utilizing NAD(P), being metabolized to 6-ANAD(P). 6-ANAD(P), in turn, can act as a competitive inhibitor of NAD(P) requiring processes. 6-ANADP is a particularly potent inhibitor of the PPP enzyme, 6-phosphogluconate (6-PG) dehydrogenase, which is an important step in the synthesis of NADPH and ribose units required for biosynthesis and DNA repair. Inhibition of this enzyme by 6-AN leads to accumulation of 6-PG which inhibits glycolysis. Therefore, ^{31}P MRS studies of tumor metabolism should detect a decrease in NTP and phosphocreatine (PCr) due to inhibition of glycolysis and possibly detect 6-PG, which is distinguishable from naturally occurring phosphoethanolamine.

Keniry *et al.* [54] used ^{31}P MRS to study 6-AN *in vitro* in combination with gossypol, another metabolic inhibitor, and found that it abolished the metabolic effects of gossypol. They were unable to resolve 6-PG in the whole cell spectra [54]. Subsequent studies have investigated the effect of 6-AN in combination with 6-methyl mercaptopurine riboside (MMPR) plus *N*-(phosphonacetyl)-L-aspartate (PALA) *in vivo*. PALA decreases pyrimidine synthesis [55], MMPR decreases purine synthesis [56], and 6-AN inhibits the PPP and glycolysis and therefore, this combination should inhibit multiple metabolic processes and enhance tumor cell kill by anti-neoplastic agents. The combination of these three drugs decreases the NTP to inorganic phosphate (P_i) ratio and the PCr to P_i ratio at 3, 10 and 24 hours [49]. Based on these findings, it was hypothesized that depletion of energy at 10 hours posttreatment with the three-drug combination would enhance response to radiation. This was evaluated by treating mice bearing first-generation transplants of the spontaneous CD8F1 mammary carcinoma with three cycles of either PALA, MMPR, and 6-AN, followed by three 15 Gy fractions, or PALA, MMPR, 6-AN, and 15 Gy given three times. This tumor model, which has a 100% correlation with human breast cancer with regards to response to chemotherapy [57], had never been cured by any previous treatments. Neither the chemotherapy nor radiation alone induced any long-term complete remissions (CR); only one brief CR was noted. However, the combination of PALA, MMPR, 6-AN, and 15 Gy given three times resulted in a 65% complete response rate with 25% of the tumor-bearing mice without recurrence at greater than 1 year, representing a likely cure of these tumors. Subsequent investigations of the effect of single-agent 6-AN as a potential radiation sensitizer *in vivo* detected 6-PG and demonstrated efficacy, although inferior to the three-drug combination [48,49].

Mechanistic studies of the effect of 6-AN on tumor metabolism were conducted in RIF-1 cells [47]. Using ^{13}C and ^{31}P MRS, perfused RIF-1 cells were studied after treatment with 40 μM 6-AN. 6-PG was detected by both ^{31}P and ^{13}C MRS (see Figure 3*A* and *B*). Figure 3*A* demonstrates ^{31}P MR spectra indicating a decrease in PCr and NTP and an increase in 6-PG after treatment with 6AN. The ^{13}C MRS studies showed that after 6-AN, 6-PG and 6-phosphoglucono-D-lactone (6-PGL) were detected (Figure 3*B*), while glucose consumption and lactate production were decreased (not shown). Enhancement of radiation only occurred when 6-AN was given before radiation and not the reverse sequence, indicating that the metabolic effect of 6-AN was necessary for radiation enhancement. It was not clear, however, whether inhibition of the pentose phosphate pathway (PPP) or glycolysis induced radiosensitization. ^{1}H MRS quantitation of the relative inhibition of glycolysis and PPP indicated that 6-AN primarily inhibited glycolysis. These studies reflect the translational potential of MR in studying metabolic inhibitors as potential anti-neoplastic agents or sensitizers [47] and as potentially valuable tools for clinical and preclinical studies.

Lonidamine

LON is a metabolic inhibitor which has been shown to enhance radiation and hyperthermia. Ben-Horin *et al.* [58] have used ^{31}P and ^{13}C MRS to study perfused MCF-7 cells. Lonidamine induced intracellular acidification accompanied by ATP depletion, decreased glucose accumulation, and increased lactate accumulation. They concluded that the mechanism of action of this drug is via inhibition of lactate transport. Ben-Yoseph *et al.* [59] studied 9L glioma cells and also noted acidosis and decreased NTP without any effect on tumor blood flow after treatment with LON. They concluded that LON inhibits lactate efflux leading to cellular acidification.

2-Deoxyglucose

2-DG is a glucose analogue that competitively inhibits both transport and metabolism of glucose. It is phosphorylated intracellularly and is thought not to undergo further metabolism and inhibits glycolysis. Karczmar *et al.* [60] have used 2-DG to deplete ATP and found that it did not affect brain bioenergetics. Kaplan *et al.* [61,62] studied

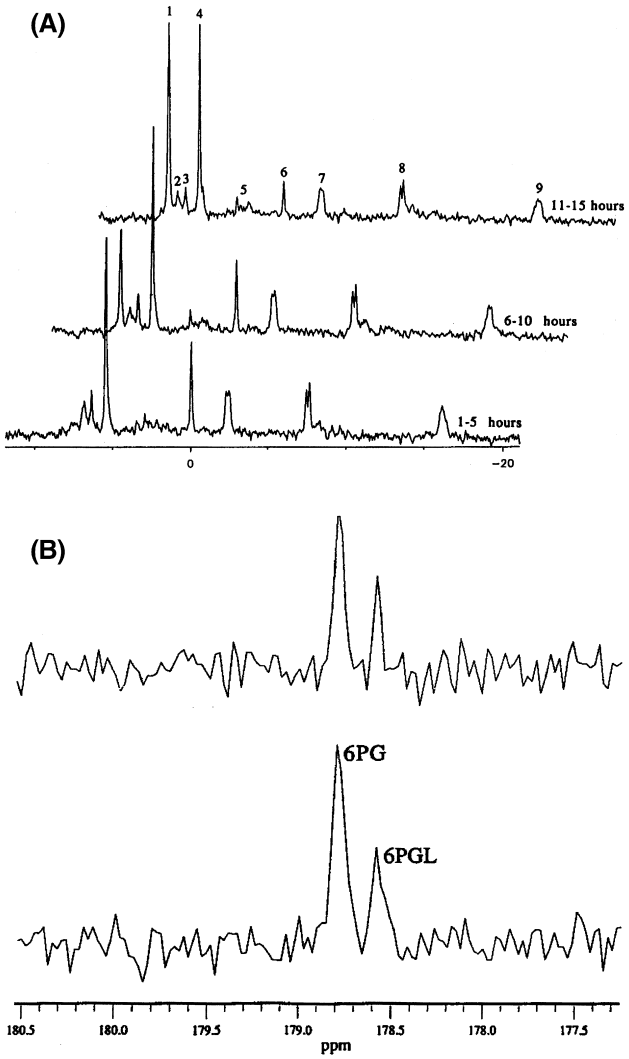

Figure 3. *(A) ^{31}P MR spectra of perfused RIF-1 tumor cells obtained during the first 1 to 5, 6 to 10 and 11 to 15 hours of perfusion with 40 μM 6-AN. Peaks are identified as follows: 1=6PG, 2=phosphoethanolamine, 3=PCho, 4=P_i, 5=phosphodiesters, 6=PCr, 7, 8, and 9 are γ-, α-, and β-NTP. Over the course of the infusion, PCr and β-NTP decrease and 6PG, which is not present initially, increases to become the dominant peak in the spectrum. Note that the P_i peak is primarily from the perfusate. (B) ^{13}C MR spectra of RIF-1 cells immediately (bottom) and 2 hours after (top) perfusion with 40 μM 6-AN and 1-^{13}C glucose. Two peaks, assigned to 6PG and 6-phosphogluconо-D-lactone, are detected both during and after perfusion and in perchloric acid extracts (not shown).*

multi-drug resistance using 2-DG. ^{13}C and ^{31}P MRS data showed that multidrug-resistant (MDR) cells accumulate more 2-DG and at a faster rate than wild-type (WT) cells. They suggested that this difference could be used therapeutically and subsequently showed that 2-DG was more toxic to MDR cells than wild type cells. In contrast, Rasmussen *et al.* [63] have also used 2-DG to study glycolytic rates and have shown that MDR Ehrlich ascites cells do not show enhanced glycolysis compared to wild type, suggesting that further studies are necessary to resolve this issue which may have therapeutic significance. Further studies to address the critical questions of selectivity and toxicity are necessary.

Influence of Tumor pH on Effectiveness of Chemotherapy

Tumors have long been known to exhibit aerobic glycolysis, generating lactic acid even in the presence of oxygen [64]. As a consequence of this phenomenon, tumors have traditionally been thought of as acidic tissues. Direct measurement of pH in a variety of solid tumors by use of microelectrodes has strengthened this viewpoint [65]. As discussed in the companion article [1], *in vivo* ^{31}P MRS permits the simultaneous non-invasive measurement of intracellular pH (pH_i) and extracellular pH (pH_e) in tumors using endogenous inorganic phosphate (P_i) and exogenous 3-aminopropylphosphonate (3-APP), respectively. Measurement of pH_i and pH_e by this method in solid tumor xenografts has shown that the pH_i of tumor cells is neutral to alkaline while the pH_e of the same tumors is acidic [66,67]. This pH gradient can impact the effectiveness of chemotherapy. The plasma membrane of cells is more permeable to the uncharged forms of ionizable drug molecules compared to their charged forms, especially for lipophilic species. Thus, while the uncharged form of the drug tends to equalize in concentration across both sides of the plasma membrane, the charged form of a weak-base species exists in higher concentration on the more acidic side of the membrane, leading to an accumulation of the drug in the more acidic compartment. This phenomenon is sometimes referred to as "ion-trapping" [68]. Cells in a tumor can maintain acid-outside plasmalemmal pH gradients of up to 0.5 pH units [69]. Some commonly prescribed antineoplastic agents, such as the anthracyclines, have acid dissociation (pK_a) constants of 7.5 to 8.5. For such drugs, acid-outside plasmalemmal pH gradients of 0.5 pH units can lead to a 50% reduction in intracellular drug levels as compared to extracellular drug levels, conferring a form of "physiological drug resistance" upon the tumor [70,71]. Abolishing or reversing the direction of the plasmalemmal pH gradient in tumors *in vivo* therefore should be an attractive means of enhancing the effectiveness of weak-base chemotherapeutic agents.

Bicarbonate can Alkalinize Tumors

Sodium bicarbonate ($NaHCO_3$) has been used in humans to treat metabolic acidosis resulting from renal failure [72] or to alleviate exercise-induced acidosis [73], and has been shown to effect modest increases in blood pH. For alkalosis to result in improved effectiveness of a weak-base drug, the subject should be able to tolerate doses of $NaHCO_3$ sufficient to produce meaningful increases in tumor pH_e. MCF7 tumor-bearing SCID mice tolerated *ad libitum* water containing 200 mM $NaHCO_3$ for periods of up to 90 days continuously and gained weight at rates similar to control mice [74]. Representative ^{31}P spectra of MCF-7 tumors grown in SCID mice treated or untreated with $NaHCO_3$ are shown in Figure 4. For the tumor in the control mouse, the pH_e measured by 3-APP is 6.93 and the pH_i measured by P_i is 7.29. In the tumor in the bicarbonate-treated mouse, the 3-APP resonance is shifted relative to controls, indicating a significant alkaliniza-

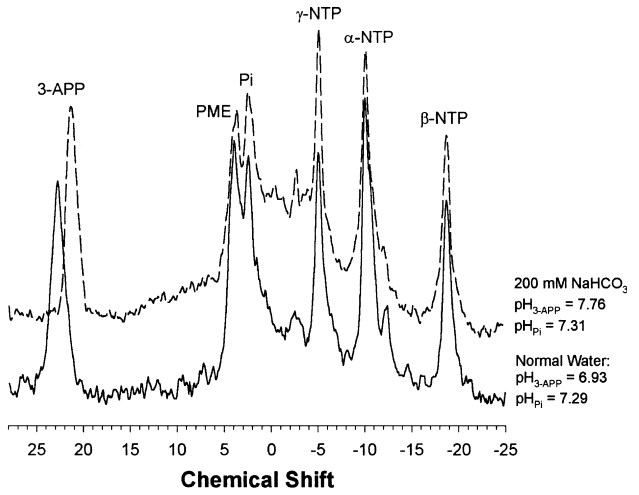

Figure 4. *^{31}P MR spectra of MCF7 tumors grown as xenografts in the mammary fat pads of female SCID mice. 3-APP: 3-aminopropylphosphonate; PME: phosphomonoesters; P_i: inorganic phosphate; NTP: nucleoside triphosphates. Representative spectra from a control mouse given normal drinking water and a mouse provided ad libitum water containing 200 mM $NaHCO_3$ are shown.*

tion of pH_e, while all other resonances (P_i, PME, NTP) are statistically indistinguishable from the control. In this example, the measured pH_e was 7.76. The maximum measured pH_e in normal hind leg tissue in bicarbonate-treated SCID mice was 7.67 compared to an average measured pH_e of 7.39 in control mice. Thus, chronic oral administration of $NaHCO_3$ resulted in significantly greater alkalinization of tumor tissue than normal tissue, and this provides a method to increase the chemotherapeutic index of weak-base drugs.

Sodium Bicarbonate Chemosensitizes Tumor Xenografts In Vivo

According to the measured plasmalemmal pH gradients, the theoretical cytosolic-to-extracellular partition ratio for doxorubicin in tumors should be 1.7 in bicarbonate-treated animals, and 0.55 in control animals, leading to a 3.1-fold increase in tumor sensitivity to doxorubicin [71]. Similarly, the calculated doxorubicin partition ratio for normal tissue is 1.9 in bicarbonate-treated animals and 1.6 in control animals, leading to a 1.2-fold increase in sensitivity of normal tissue to doxorubicin. Thus, bicarbonate treatment can potentially yield a 2.6-fold increase in the chemotherapeutic index of doxorubicin. Indeed, combination therapy of MCF7 tumor-bearing SCID mice with doxorubicin and 200 mM $NaHCO_3$ resulted in a significantly reduced tumor growth rate in those mice as compared to tumors in mice treated with doxorubicin alone, while bicarbonate alone had no effect on the tumor growth rate [74]. Prolonged treatment with sodium bicarbonate in the drinking water did not have significant effects on animal well being. In mice, the lifetime of free drug is on the order of 1 hour following intravenous delivery [75]. Therefore, acute metabolic alkalinization with sodium bicarbonate lasting 1–2 hours should enhance drug uptake into tumor cells while sparing the host animal the deleterious effects of chronic denial of fresh water. For the very same reasons, acute alkalinization should also have greater clinical utility than chronic treatment with sodium bicarbonate.

Radiation and Tumor Oxygenation

Measurements of tumor oxygenation and changes in tumor oxygenation are crucial to an understanding of tumor physiology and response to therapy. The oxygen tension in tumors is a key determinant of the sensitivity of tissues to ionizing radiation and to certain chemotherapeutic agents [76]. For many years, the occurrence of hypoxia in tumors has been postulated to be a limiting factor in the response to radiation therapy [77] and recent results using the Eppendorf electrode system to measure pO_2 have confirmed that this can occur in human tumors [78,79]. In addition to quantitative oxygen measurements made using oxygen electrodes, a variety of spectroscopic methods have been used. Some of these are based on the use of fluorescent and phosphorescent probes which are sensitive to oxygen tension. Others are based on spectroscopic differences between deoxyhemoglobin and oxyhemoglobin. Although these methods offer some advantages, none of them is used routinely and their invasiveness and/or poor spatial resolution has encouraged increased emphasis on the development of magnetic resonance methods sensitive to oxygen tension.

Some magnetic resonance methods are quantitative, directly measure tumor pO_2, and may allow identification of hypoxic tumor regions and accurate measurement of changes in pO_2 during therapy. One very promising method is based on ^{19}F MRI of signals from perfluorocarbons after either intravenous or intratumoral injection [80,81]. As described in the companion review [1], the T_1 relaxation time of the fluorine nucleus in these molecules is sensitive to local oxygen tension, and since relatively large amounts of fluorine-containing molecules can be injected, images with reasonable spatial resolution can be obtained. Another approach, *in vivo* electron paramagnetic resonance (EPR) oximetry with particulate materials, can provide repeated non-perturbing measurements from the same site [82]. EPR oximetry is based on the fact that the presence of molecular oxygen affects the linewidth of paramagnetic materials. This effect is especially useful in lines that are intrinsically narrow or have mechanisms that involve factors in addition to those mediated simply by changes (decreases) in relaxation times. The effects of oxygen on linewidths of carbon-based particulates derived from coals or chars are especially large at low concentrations of oxygen, making these materials particularly suitable for oximetry in tumors where the pO_2 values of most interest are quite low (in the range of 0 to 10 Torr).

Another MR approach, which makes use of proton (water) MRI, relies on blood-oxygen-level-dependent (BOLD) contrast. The large paramagnetic susceptibility of deoxyhemoglobin generates large magnetic field gradients in and around blood vessels which effect the linewidth (or

T_2* relaxation time) of the water proton signal. This does not allow quantitative measurement of the oxygen level, except in large veins, because there are many other important influences on the water proton signal. However, BOLD MRI can provide a qualitative indication of changes in tumor oxygenation. Equipment used to obtain BOLD MRI measurements is widely available both for clinical measurements in cancer patients and for studies of animal models.

Tumor Reoxygenation

A dose of radiation kills oxygenated cells more efficiently, leaving a greater proportion of hypoxic cells that tend to reoxygenate in many animal tumors and human xenografts [83]. It has been suggested that one of the reasons fractionated radiation is successful is that tumor reoxygenation occurs after each dose. Consequently, the tumor is well-oxygenated at the time of subsequent doses, while the effects on normal tissues are not altered because they already are fully oxygenated in terms of responses to radiation [84]. Different tumor types and different individual tumors, however, may fail to reoxygenate or may have altered timing of post-radiation changes in pO_2. It then follows that if methods were available to assess tumor oxygenation status repeatedly and accurately, more effective radiation treatments could be carried out by timing radiation doses to take advantage of reoxygenation. Those tumors that fail to reoxygenate and thus are unlikely to respond to irradiation could be treated with another modality without having to wait for the current endpoint, which is a failure to respond adequately to the full course of therapy.

Using EPR oximetry, the time course of pO_2 changes after an initial radiation dose in animal tumors has been followed over periods of several weeks [85]. The typical time pattern after irradiation has been an initial decrease post-irradiation, followed by a subsequent increase in tumor pO_2. The biological significance for these changes was tested by delivering split-dose radiation with the second dose timed to coincide with the measured high or low point of pO_2 post-irradiation (see Figure 5). As shown in the figure, the measured values of pO_2 were predictive of the biological effect. In fact, the effects of the split-dose regime delivered at the time when the pO_2 was at its high point post-irradiation was at least as effective as if the radiation had been delivered in a single dose, even though usually splitting a dose of radiation lowers its efficacy.

These results suggest that EPR oximetry may be a useful tool for optimizing the scheduling of radiation therapy by enabling the therapist to deliver radiation doses at times where the maximum effects would occur in the tumors. Because at normal (physiological) levels of oxygen the radiation response of cells does not change over a broad range of oxygen concentrations and surrounding normal tissues usually do not have hypoxic areas, the response of the normal tissues adjacent to the tumor is not affected by radiation-induced changes in the pO_2. Therefore, by optimizing the scheduling of radiation to coincide with post-irradiation increases of oxygenation, the therapeutic ratio should be increased.

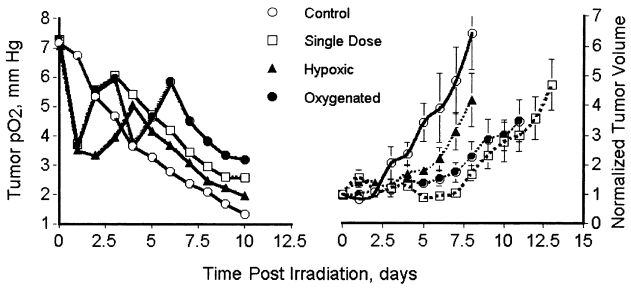

Figure 5. *Effects of radiation on pO_2 and volume of tumors. Twenty Gy of ionizing radiation was given as a single dose or as a split dose with the interval between the two 10 Gy doses determined by the time course of changes in mean tumor pO_2. Treatment groups were: ○ - Control (Sham - Irradiated); □ - Single (20 Gy at time 0); ● - Oxygenated (10 Gy at time 0 and 10 Gy at 72 hours); ▲ - Hypoxic (10 Gy at time 0 and 10 Gy at 24 hours). Points are the mean of five mice per group; error bars are SEM of measurements from five tumors at each time point. Left side: Changes in pO_2 as measured by EPR oximetry. Right side: Tumor volume as determined by physical measurements of three axes (revised from Ref. [85]).*

While these results are quite promising, additional studies in animals and then in human patients will be required to demonstrate the efficacy of this approach. Other techniques that could provide similar data (e.g., ^{19}F MRI with perfluorocarbons) would be equally applicable; however, their capability to assess reoxygenation has not been established. The EPR technique described above can be extended to report on the pO_2 in several locations simultaneously by the use of suitable gradients of the magnetic field [86]. Using soluble stable free radicals, it may be possible to obtain much more detailed maps of pO_2 in tumors using EPR imaging [87].

Modifiers of Tumor Oxygenation

Although tumor reoxygenation may lead to effective radiotherapy in some tumors, in others, treatments designed to increase tumor oxygenation may be required. Because the efficacy of tumor-oxygenating treatments likely varies among tumors, non-invasive methods to assess their impact are needed to guide their development and clinical use. Several laboratories have used BOLD MRI to detect large and reproducible T_2* increases in a number of rodent tumor models during inhalation of pure oxygen and carbogen [88–93]. In at least one tumor model, the R3230 mammary adenocarcinoma growing in Fisher rats changes in T_2* during tumor-oxygenating treatments averaged over the whole tumor strongly correlates with changes measured with an oxygen microelectrode (Ref. [92]; see Figure 6). Moreover, in BA1112 tumors, BOLD MRI correctly ranks the effects of three tumor-oxygenating treatments [carbogen alone, perfluorocarbon (PFC) emulsion injected intravenously, and the combination of carbogen and PFC] on tumor hypoxic fraction [91]. This experimental evidence supports the hypothesis that changes in T_2* reflect changes in the oxygen saturation of blood in tumors caused by tumor-oxygenating treatments — and that this is strongly related to changes in extravascular pO_2 and hypoxic fraction.

MRI allows evaluation of spatial and temporal heterogeneity within tumors in their response to oxygenating

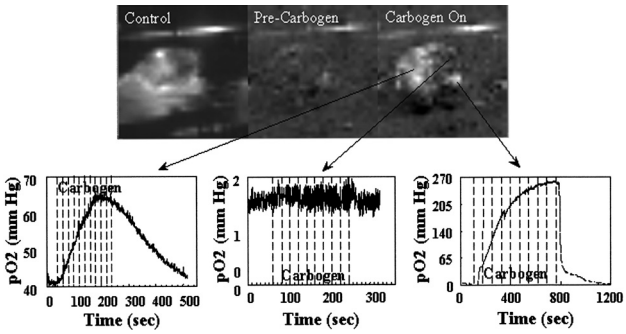

Figure 6. *Correlation of MR and oxygen microelectrode data: Water signal peak height in a rodent mammary adenocarcinoma under control conditions. The subsequent images show the difference between control images and the change in water signal peak height during carbogen breathing. The changes are spatially inhomogeneous and occur primarily in the tumor. The graphs below show changes in pO_2 measured by oxygen microelectrode during carbogen breathing in the same tumor. The region in which MR signal peak height does not change also shows no change in microelectrode current*

treatments. In fact, MRI has provided some evidence that some tumor regions respond paradoxically to oxygenating treatments. Although there may be an increase in average oxygenation, tumor-oxygenating treatments frequently decrease blood oxygenation in a small but significant fraction of tumor volume as indicated by increased water signal linewidth [92]. This may mean that some tumor regions become more radioresistant during tumor-oxygenating treatments, and cells in these regions may survive radiation and repopulate the tumor following therapy. Depending on the mechanism underlying these effects, MRI could guide the formulation of tumor-oxygenating treatments or combinations of tumor-oxygenating treatments which maximally increase oxygenation throughout the entire tumor volume.

Oxygen challenges cause contrast changes in MRI images which may be useful for diagnostic purposes. Decreases in water signal linewidth in tumors caused by tumor-oxygenating treatments are much more significant than changes in surrounding normal tissues [Refs. [88,89]; e.g., see Figure 6]. This may be because tumors are initially hypoxic while normal tissue is not. Conversely, Vexler *et al.* [94] showed that decreases in T_2^* in rodent hepatic tumors due to ischemia are much larger than T_2^* decreases in surrounding normal tissue; perhaps because the tumors have insufficient blood supply. Thus, changes in T_2^* in response to increases or decreases in blood oxygenation may help to identify tumor regions which are hypoxic or on the verge of hypoxia. In general, changes in image contrast in response to a variety of benign challenges, which affect oxygenation and blood supply, may help to identify tumors and characterize their physiology.

Use of EPR and MRI to measure tumor oxygenation and changes in tumor oxygenation is a relatively new field that is developing rapidly. The methods that are now being developed and validated may have a significant impact on the diagnosis and treatment of solid tumors in the coming decade.

Gene Therapy

Gene therapy offers the possibility of curing disease by correcting the genetic defects that underlie its pathogenesis. As a genetic disease caused by multiple mutations in growth-regulating genes in a single cell, cancer does not seem amenable to this form of "corrective" gene therapy. However, there has arguably been more success in cancer gene therapy than any other type. There are currently over 200 cancer gene therapy protocols enrolling patients. The majority of these novel therapeutic approaches do not aim to correct the host of somatic mutations that lead to oncogenesis, but rather aim to create therapeutically exploitable phenotypic differences between normal and malignant cells.

Two of the most widely studied cancer gene therapy paradigms rely on expression of non-mammalian enzymes that convert non-toxic prodrugs into cytotoxic metabolites. Local expression of such prodrug-converting enzymes in tumor tissue results in localized chemotherapy, aiming to improve outcomes by minimizing the dose-limiting toxicity associated with systemic chemotherapy. The first of these "chemosensitization" gene therapy approaches is based on the preferential phosphorylation of the anti-herpetic drug, ganciclovir, by the Herpes Simplex Virus thymidine kinase (HSV-*tk*) gene [95]. The other widely employed strategy results in the production of the antimetabolite, 5-FU, from the antimycotic agent, 5-fluorocytosine (5-FC), by the enzymatic action of microbial cytosine deaminase (CD) [96].

Imaging of Transgene Expression

The ability to non-invasively measure the distribution, magnitude and duration of therapeutic transgene expression could have a profound impact on the development of cancer gene therapy. Such assays would allow subject-by-subject correlation of therapeutic efficacy with levels of transgene expression, as was recently accomplished using radionuclide imaging [97], and would be useful tools in the development of vector technology. A recent study has demonstrated the potential of MR spectroscopy for visualizing transgene expression in cancer cells [98]. In this study, the enzymatic activity of yeast CD expressed in subcutaneous tumors was quantified with ^{19}F MRS to observe the conversion of 5-FC to 5-FU. This study was the first direct confirmation that an enzyme/prodrug gene therapy paradigm results in local chemotherapy (see Figure 7). Future studies may provide data on the feasibility of obtaining ^{19}F MR images of the metabolites within the tumor tissue that would allow for regional assessment of CD delivery for correlation with therapeutic response.

While a variety of delivery vehicles have been utilized for delivering transgenes to tumor cells, viral vectors have been the most widely used vector systems. Viral vectors have similar dimensions as monocrystalline iron oxide (MION) particles which are used as an MRI contrast agent. MR has been reported useful for imaging the distribution of viral vectors as they have been shown to have essentially the same tissue distribution as MION particles [99]. Additional

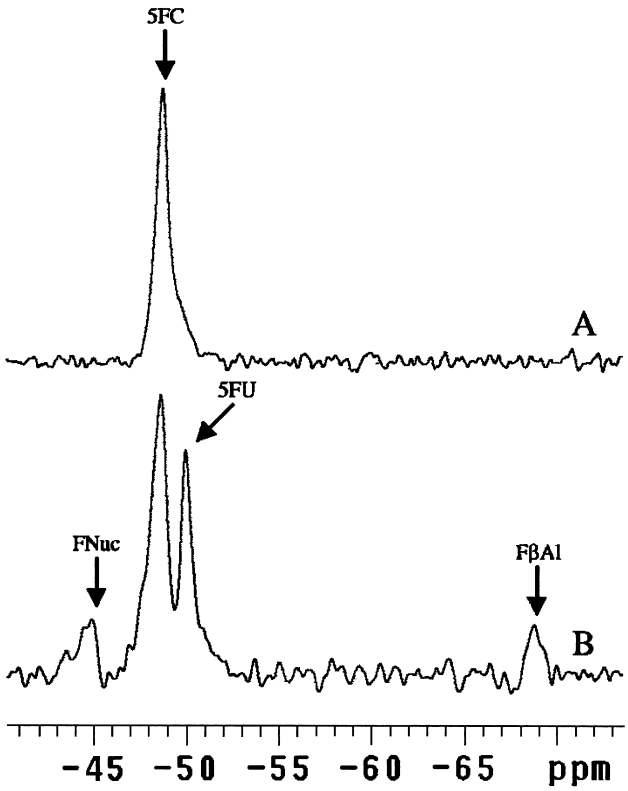

Figure 7. *Representative in vivo ^{19}F spectra from subcutaneous tumors obtained 120–150 minutes following i.p. injection of 1 g kg^{-1} 5-FC. A single peak of 5-FC is observed in the parental HT29 carcinoma (A). In contrast, the HT29 carcinoma expressing yCD (B) converted the 5-FC to 5-FU, which was subsequently metabolized into fluorinated nucleotides (Fnuc). Fluoro-β-alanine (FβAl), a catabolic breakdown product of 5-FU, was also observed in this tumor. Reprinted from Stegman L.D. et al. [98]. Non-invasive detection of cytosine deaminase transgene expression in human tumor xenografts with in vivo magnetic resonance spectroscopy [PNAS **96**: 9821–9826. National Academy of Sciences, U.S.A. Copyright (1999).]*

strategies for using MRI to detect gene delivery have been demonstrated *in vitro* using specific marker genes such as melanin [100] and the human transferrin receptor [101].

Therapeutic Assessment of Gene Therapy

Small animal tumor models are used for the pre-clinical evaluation of the anti-neoplastic efficacy of experimental gene therapy paradigms. The use of MRI and MRS for evaluating the effects of gene therapy on tumor physiology, biology, biochemistry, and morphology has been reported. Studies using orthotopic tumor models have benefited from the use of MR, which provides the ability to demarcate the location and size of the tumor prior to gene delivery. This has been used for the guiding the delivery of both retroviral [102] and adenoviral [103] vectors into intracerebral glioma models. Changes in tumor volumes and growth rates following gene therapy protocols in orthotopic tumor models have also proven beneficial for assessing therapeutic efficacy [96,103–106]. In addition to using MR to assess changes in morphometry, recent studies using diffusion MRI (see Early Detection of Therapeutic Response section) have shown that changes in tumor water ADC can be observed following gene therapy [32,33]. Finally, changes in MRS-observable proton metabolites following HSV-*tk* gene therapy have also been reported [32,103]. Taken together, these studies reveal that a variety of significant gene therapy-induced effects can be non-invasively observed in tumor models using MRI/S.

Anti-Vascular Therapy

Anti-vascular cancer therapy is here defined as a treatment acting primarily via effects on development or function of tumor blood vessels. Its potential advantages include the following. 1) Damage to a small number of vascular endothelial cells could result in the death of a large number of tumor cells which depend on them for the supply of nutrients. 2) It is easier to deliver drugs to vascular endothelial cells than to cells in solid tumors. 3) Tumor vasculature is a new target so agents should have a new spectrum of toxicities. 4) Inhibition of formation of new blood vessels (anti-angiogenic therapy) may slow or prevent metastatic spread or growth of micro-metastases. Because MR can non-invasively assess tumor vascularity and energetics, it provides a powerful tool for the pre-clinical development of anti-vascular therapy that can be readily translated into clinical use.

Vaso-Active Agents

Several vaso-active agents, in particular hydralazine, have been shown to result in a selective reduction in tumor perfusion in transplanted animal tumors and, in some cases, also in primary tumors in animals [e.g. Ref. [107]]. ^{31}P MRS has been widely applied in such studies for non-invasive monitoring of the metabolic consequences of an acute reduction in tumor blood flow (fall in NTP, increase in P_i and often a decrease in pH). The mechanism of action is generally believed to involve vasodilatation of normal peripheral blood vessels, resulting in a reduction in arterial blood pressure and a "steal effect" of blood away from the tumor (tumor vessels may not respond normally because of a lack of smooth muscle and/or appropriate receptors). The high interstitial pressure of tumors may also contribute to the collapse of some vessels when blood pressure falls. Since the blood flow and metabolic effects of this approach are generally short-lived and do not normally cause permanent damage to tumor blood vessels, they are not normally included as anti-vascular agents.

Cytokines and Cytokine-Releasing Agents

Vascular damage has been shown to be an important feature of treatments with the cytokines TNF-α [108] and IL-1α [109]. These cytokines resulted in hemorrhage (determined histologically) and an attenuation of tumor energetic status (^{31}P MRS). Flavone acetic acid (FAA) was probably the first anti-cancer drug shown to act predominantly via tumor vascular damage. Evelhoch *et al.* [110] demonstrated that FAA caused a reduction in bioenergetic

status (^{31}P MRS measurement of NTP/P_i) and in tumor blood flow (^{2}H MRS measurement of D_2O clearance). Su *et al.* [44] measured the uptake of Gd-DTPA and a macromolecular MR contrast agent (gadomer-17, 35 kDa) in a rat adenocarcinoma before treatment and after a combination of Mitomycin-C and FAA. The kinetics of Gadomer-17 was used to calculate tumor vascular volume, which was reduced by 42% 4 days after treatment in responding tumors. Unfortunately, the pre-clinical success with FAA was not translated into the clinic, possibly because FAA acted via causing a release of TNF in the mouse but did not lead to TNF release in humans. A more potent analogue of FAA, dimethylxanthenone acetic acid (DMXAA), has been developed which can cause TNF release in humans. ^{31}P MRS has been used to follow the time course and dose-dependency of DMXAA effects in murine C3H mammary tumors [111] while DCE-MRI studies (uptake of Gd-DTPA) have been included in phase I clinical trials of DMXAA and preliminary results showed a reduction in both the rate and magnitude of Gd-DTPA uptake 24 hours post-treatment in 7 out of 10 patients [112].

Tubulin-Binding Agents

Combretastatin is a tubulin-binding agent with anti-angiogenic and anti-vascular properties. Beauregard *et al.* [113] used ^{31}P MRS and several MRI approaches to study the effects of combretastatin (100 mg kg^{-1}) on subcutaneous sarcoma F tumors in mice. They observed a fall in energetic status (reported as a two-fold increase in P_i/NTP) 150 minutes after treatment and a fall in tumor pH. The rate of uptake of Gd-DTPA into the tumor center was decreased 2.5-fold at 160 minutes with a smaller effect reported for the tumor periphery. Changes in T_2-weighted images (i.e., slight increases in the area of low signal intensity regions) 180 minutes after treatment were ascribed to hemorrhage, consistent with histological changes in these tumors. The tumor water ADC was measured before and up to 1.8 hours after treatment but no significant changes were detected. Maxwell *et al.* [114] used MRS and MRI techniques to study the effects of combretastatin (100 mg kg^{-1}) on C3H mammary tumors implanted on the mouse foot. The ^{31}P MRS results were similar to those of Beauregard *et al.* [113] (marked fall in NTP/P_i) although an additional measurement at 24 hours after treatment showed full recovery of NTP/P_i. Single-voxel ^{1}H MRS measurements of lactate did not show a consistent increase, possibly due to lipid contamination and/or a reduction in glucose supply associated with blood flow reduction. No increase in low signal intensity regions of T_2-weighted MR images was detected within 3 hours of combretastatin treatment. In the case of the C3H mammary tumor, histology showed no significant increase in tumor necrosis 3 hours after treatment although an increase in necrosis from 2% to 16% was observed at 24 hours. The extent of hemorrhagic necrosis may vary between anti-vascular therapies and tumor types but these data imply that hemorrhage is not a pre-requisite for combretastatin-induced tumor blood flow reduction.

Future Development of Anti-Vascular Agents

Given the availability of MR methods relevant to the actions of anti-vascular drugs, it is both feasible and desirable to include MR end points as part of the pre-clinical and clinical evaluation of such agents. However, several complicating factors should be taken into account. 1) The analysis of Gd-DTPA kinetics may be complicated by drugs which act both to decrease perfusion and to increase vascular permeability. Freely diffusible tracers (e.g. D_2O for animal studies) and blood-pool contrast agents may give more specific information. 2) Conflicting effects of hemorrhagic necrosis and edema may be seen in MR images. 3) Lacate-edited ^{1}H MRS is relatively sensitive and specific but lactate changes may be attenuated by limited glucose supply. 4) ^{31}P MRS is relatively insensitive but has been valuable for monitoring the effects of vaso-active and vascular-damaging agents in animal tumors. There may be a threshold of blood flow reduction and/or a delay before effects on energy metabolism are observed. 5) A range of MRI tools for studying angiogenesis has been introduced [e.g., Abramovitch *et al.* [115], Sipkins *et al.* [116]] and may be useful for evaluating anti-angiogenic drugs. High spatial resolution will be needed and micro-metastases may be difficult or impossible (at the present time) to detect.

Summary

Magnetic resonance can non-invasively provide a wealth of information regarding tumor metabolism and pathophysiology. As a consequence, it has contributed to our understanding of both the effects of treatment on tumor metabolism and pathophysiology and the importance of tumor metabolism and pathophysiology as determinants of therapeutic response. MR has made substantial contributions in these areas including several discussed in this review. MR can readily monitor changes such as cell shrinkage, already known to occur during apoptosis, and previously unappreciated metabolic changes associated with upstream steps in the apoptotic pathway have been identified. MR measurable changes in tumor water ADC induced by cytotoxic therapy, which appear to be associated with changes in tumor pathophysiology due to cell death, may be generally applicable for early detection of response to cytotoxic therapy. DCE-MRI is a practical tool for non-invasive evaluation of changes in tumor vascularity following cancer therapy and may provide an early indication of therapeutic response. The metabolic information provided by MR allows evaluation of the pharmacodynamics of metabolic inhibitors that can help to optimize their use as potential anti-neoplastic agents or sensitizers. ^{31}P MRS measurement of pH_e and pH_i simultaneously demonstrates for the first time *in vivo* that raising the plasmalemmal pH gradient with sodium bicarbonate in drinking water leads to significant improvements in the therapeutic effectiveness of doxorubicin against MCF-7 xenografts. Non-invasive assessment of tumor oxygenation with EPR and MRI allows the effects of modulating hypoxia to be considered in the timing of

subsequent doses of radiotherapy. ^{19}F MRS quantitation of the enzymatic activity of yeast CD expressed in subcutaneous tumors by observing the conversion of 5-FC to 5-FU is the first direct confirmation that an enzyme/prodrug gene therapy paradigm results in local chemotherapy. Because *in vivo* tumor metabolism and pathophysiology can be assessed non-destructively by MR, pre-clinical results from cellular or animal models are often easily translated into the clinic. Hence, these MR techniques, which have distinct advantages over other proposed and currently implemented techniques, have the potential to revolutionize treatment monitoring.

References

[1] Gillies RJ, Bhujwalla ZM, Evelhoch JL, Garwood M, Neeman M, Robinson SP, Sotak CH, and van der Sanden B (2000). Applications of magnetic resonance in model systems: tumor biology and physiology. *Neoplasia* **2**, 139–152.

[2] Kerr JF, Wyllie AH, and Currie AR (1972). Apoptosis: a basic biological phenomenon with wide-ranging implications in tissue kinetics. *Br J Cancer* **26**, 239–257.

[3] Miller LJ, and Marx J (1998). Apoptosis. *Science* **281**, 1301.

[4] Hickman JA (1992). Apoptosis induced by anticancer drugs. *Cancer Metastasis Rev* **11**, 121–139.

[5] Pilatus U, Shim H, Artemov D, Davis D, van Zijl PC, and Glickson JD (1997). Intracellular volume and apparent diffusion constants of perfused cancer cell cultures, as measured by NMR. *Magn Reson Med* **37**, 825–832.

[6] Pfeuffer J, Flogel U, and Leibfritz D (1998). Monitoring of cell volume and water exchange time in perfused cells by diffusion-weighted ^{1}H NMR spectroscopy. *NMR Biomed* **11**, 11–18.

[7] Blankenberg FG, Storrs RW, Naumovski L, Goralski T, and Spielman D (1996). Detection of apoptotic cell death by proton nuclear magnetic resonance spectroscopy. *Blood* **87**, 1951–1956.

[8] Hakumaki JM, Poptani H, Sandmair AM, Yla-Herttuala S, and Kauppinen RA (1999). ^{1}H MRS detects polyunsaturated fatty acid accumulation during gene therapy of glioma: implications for the *in vivo* detection of apoptosis. *Nat Med* **5**, 1323–1327.

[9] Al-Saffar NM, Clarke PA, DiStefano F, Leach MO, and Ronen SM (1999). Detection of Metabolic Changes Associated with Fas- and Chemotherapy-Induced Apoptosis Using MRS. In *ISMRM 7th Scientific Meeting*. ISMRM, Philadelphia, PA.

[10] Anthony ML, Zhao M, and Brindle KM (1999). Inhibition of phosphatidylcholine biosynthesis following induction of apoptosis in HL-60 cells. *J Biol Chem* **274**, 19686–19692.

[11] Adebodun F, and Post JF (1994). ^{31}P NMR characterization of cellular metabolism during dexamethasone induced apoptosis in human leukemic cell lines. *J Cell Physiol* **158**, 180–186.

[12] Ronen SM, DiStefano F, McCoy CL, Robertson D, Smith TA, Al-Saffar NM, Titley J, Cunningham DC, Griffiths JR, Leach MO, and Clarke PA (1999). Magnetic resonance detects metabolic changes associated with chemotherapy-induced apoptosis. *Br J Cancer* **80**, 1035–1041.

[13] Williams SN, Anthony ML, and Brindle KM (1998). Induction of apoptosis in two mammalian cell lines results in increased levels of fructose-1,6-bisphosphate and CDP-choline as determined by ^{31}P MRS. *Magn Reson Med* **40**, 411–420.

[14] Bogin L, Papa MZ, Polak-Charcon S, and Degani H (1998). TNF-induced modulations of phospholipid metabolism in human breast cancer cells. *Biochim Biophys Acta* **1392**, 217–232.

[15] Nunn AV, Barnard ML, Bhakoo K, Murray J, Chilvers EJ, and Bell JD (1996). Characterisation of secondary metabolites associated with neutrophil apoptosis. *FEBS Lett* **392**, 295–298.

[16] Dahan-Grobgeld E, Maragalit R, and Degani H (1995). Elevation in the Nucleotidetriphophate Pool of Human Breast Cancer Cells Precedes Apoptosis Induced by Adriamycin: Studies by ^{31}P MRS and Immunohistochemistry. In *ISMRM 3rd Scientific Meeting*. ISMRM, Nice, France.

[17] Boddie AW, Jr., Constantinou A, Williams C, and Reed A (1998). Nitrogen mustard upregulates Bcl-2 and GSH and increases NTP and PCr in HT-29 colon cancer cells. *Br J Cancer* **77**, 1395–1404.

[18] Ellis PA, Smith IE, McCarthy K, Detre S, Salter J, and Dowsett M (1997). Preoperative chemotherapy induces apoptosis in early breast cancer [letter]. *Lancet* **349**, 849.

[19] Stejskal EO, and Tanner JE (1965). Spin diffusion measurements: spin echoes in the presence of a time-dependent field gradient. *J Chem Phys* **42**, 288–292.

[20] Cooper RL, Chang DB, Young AC, Martin CJ, and Ancker-Johnson D (1974). Restricted diffusion in biophysical systems. Experiment. *Biophys J* **14**, 161–177.

[21] Latour LL, Svoboda K, Mitra PP, and Sotak CH (1994). Time-dependent diffusion of water in a biological model system. *Proc Natl Acad Sci USA* **91**, 1229–1233.

[22] Peterson HI, Appelgren L, Kjartansson I, and Selander D (1976). Vascular and extravascular spaces in a transplantable rat tumour after local X-ray irradiation. *Zeitschrift fur Krebsforschung und Klinische Onkologie— Cancer Research and Clinical Oncology* **87**, 17–25.

[23] Braunschweiger PG (1988). Effect of cyclophosphamide on the pathophysiology of RIF-1 solid tumors. *Cancer Res* **48**, 4206–4210.

[24] Le Bihan D, Breton E, Lallemand D, Grenier P, Cabanis E, and Laval-Jeantet M (1986). MR imaging of intravoxel incoherent motions: application to diffusion and perfusion in neurologic disorders. *Radiology* **161**, 401–407.

[25] Brunberg JA, Chenevert TL, McKeever PE, Ross DA, Junck LR, Muraszko KM, Dauser R, Pipe JG, and Betley AT (1995). *In vivo* MR determination of water diffusion coefficients and diffusion anisotropy: correlation with structural alteration in gliomas of the cerebral hemispheres [published erratum appears in *AJNR Am J Neuroradiol* **16** (6), 1384: 1995 Jun–Jul]. *AJNR Am J Neuroradiol* **16**, 361–371.

[26] Englander SA, Ulug AM, Brem R, Glickson JD, and van Zijl PC (1997). Diffusion imaging of human breast. *NMR Biomed* **10**, 348–352.

[27] Namimoto T, Yamashita Y, Sumi S, Tang Y, and Takahashi M (1997). Focal liver masses: characterization with diffusion-weighted echo-planar MR imaging. *Radiology* **204**, 739–744.

[28] Yamashita Y, Namimoto T, Mitsuzaki K, Urata J, Tsuchigame T, Takahashi M, and Ogawa M (1998). Mucin-producing tumor of the pancreas: diagnostic value of diffusion-weighted echo-planar MR imaging. *Radiology* **208**, 605–609.

[29] Namimoto T, Yamashita Y, Mitsuzaki K, Nakayama Y, Tang Y, and Takahashi M (1999). Measurement of the apparent diffusion coefficient in diffuse renal disease by diffusion-weighted echo-planar MR imaging. *J Magn Reson Imaging* **9**, 832–837.

[30] Zhao M, Pipe JG, Bonnett J, and Evelhoch JL (1996). Early detection of treatment response by diffusion-weighted ^{1}H NMR spectroscopy in a murine tumour *in vivo*. *Br J Cancer* **73**, 61–64.

[31] Chenevert TL, McKeever PE, and Ross BD (1997). Monitoring early response of experimental brain tumors to therapy using diffusion magnetic resonance imaging. *Clin Cancer Res* **3**, 1457–1466.

[32] Hakumaki JM, Poptani H, Puumalainen AM, Loimas S, Paljarvi LA, Yla-Herttuala S, and Kauppinen RA (1998). Quantitative ^{1}H nuclear magnetic resonance diffusion spectroscopy of BT4C rat glioma during thymidine kinase-mediated gene therapy *in vivo*: identification of apoptotic response. *Cancer Res* **58**, 3791–3799.

[33] Poptani H, Puumalainen AM, Grohn OH, Loimas S, Kainulainen R, Yla-Herttuala S, and Kauppinen RA (1998). Monitoring thymidine kinase and ganciclovir-induced changes in rat malignant glioma *in vivo* by nuclear magnetic resonance imaging. *Cancer Gene Ther* **5**, 101–109.

[34] Galons J-P, Altbach MI, Taylor CW, Payne-Murrietta G, and Gillies RJ (1999). Early increases in breast tumor xenograft water mobility in response to paclitaxel therapy detected by non-invasive diffusion magnetic resonance imaging. *Neoplasia* **1**, 113–117.

[35] Lemaire L, Howe FA, Rodrigues LM, and Griffiths JR (1999). Assessment of induced rat mammary tumour response to chemotherapy using the apparent diffusion coefficient of tissue water as determined by diffusion-weighted ^{1}H NMR spectroscopy *in vivo*. *Magma* **8**, 20–26.

[36] He Z (1999). Tumor therapeutic response detected by nuclear magnetic resonance diffusion measurement. PhD Dissertation, Wayne State University.

[37] Corbett TH, and Valeriote FA (1987). Rodent Models in Experimental Chemotherapy. In *Rodent Tumor Models in Experimental Cancer Therapy*. RF Kallman (Ed). Pergamon Press, New York. pp. 233–252.

[38] Kuhl CK, Mielcareck P, Klaschik S, Leutner C, Wardelmann E, Gieseke J, and Schild HH (1999). Dynamic breast MR imaging: are

signal intensity time course data useful for differential diagnosis of enhancing lesions? *Radiology* **211**, 101–110.

[39] Hulka CA, Edmister WB, Smith BL, Tan L, Sgroi DC, Campbell T, Kopans DB, and Weisskoff RM (1997). Dynamic echo-planar imaging of the breast: experience in diagnosing breast carcinoma and correlation with tumor angiogenesis. *Radiology* **205**, 837–842.

[40] Mayr NA, Yuh WT, Zheng J, Ehrhardt JC, Magnotta VA, Sorosky JI, Pelsang RE, Oberley LW, and Hussey DH (1998). Prediction of tumor control in patients with cervical cancer: analysis of combined volume and dynamic enhancement pattern by MR imaging. *AJR Am J Roentgenol* **170**, 177–182.

[41] Hawighorst H, Weikel W, Knapstein PG, Knopp MV, Zuna I, Schonberg SO, Vaupel P, and van Kaick G (1998). Angiogenic activity of cervical carcinoma: assessment by functional magnetic resonance imaging-based parameters and a histomorphological approach in correlation with disease outcome. *Clin Cancer Res* **4**, 2305–2312.

[42] Schwickert HC, Stiskal M, Roberts TP, van Dijke CF, Mann J, Muhler A, Shames DM, Demsar F, Disston A, and Brasch RC (1996). Contrast-enhanced MR imaging assessment of tumor capillary permeability: effect of irradiation on delivery of chemotherapy. *Radiology* **198**, 893–898.

[43] Cohen FM, Kuwatsuru R, Shames DM, Neuder M, Mann JS, Vexler V, Rosenau W, and Brasch RC (1994). Contrast-enhanced magnetic resonance imaging estimation of altered capillary permeability in experimental mammary carcinomas after X-irradiation. *Invest Radiol* **29**, 970–977.

[44] Su MY, Wang Z, and Nalcioglu O (1999). Investigation of longitudinal vascular changes in control and chemotherapy-treated tumors to serve as therapeutic efficacy predictors. *J Magn Reson Imaging* **9**, 128–137.

[45] Hellman S (1993). Principles of Chemotherapy. In *Cancer: Principles and Practice of Oncology*. VT DeVita, S Hellman, and SA Rosenberg (Eds). JB Lippincott Co., Philadelphia, PA. p. 255.

[46] Street JC, Mahmood U, Ballon D, Alfieri AA, and Koutcher JA (1996). ^{13}C and ^{31}P NMR investigation of effect of 6-aminonicotinamide on metabolism of RIF-1 tumor cells *in vitro*. *J Biol Chem* **271**, 4113–4119.

[47] Street JC, Alfieri AA, and Koutcher JA (1997). Quantitation of metabolic and radiobiological effects of 6-aminonicotinamide in RIF-1 tumor cells *in vitro*. *Cancer Res* **57**, 3956–3962.

[48] Koutcher JA, Alfieri AA, Matei C, Meyer KL, Street JC, and Martin DS (1996). Effect of 6-aminonicotinamide on the pentose phosphate pathway: ^{31}P NMR and tumor growth delay studies. *Magn Reson Med* **36**, 887–892.

[49] Koutcher JA, Alfieri AA, Stolfi RL, Devitt ML, Colofiore JR, Nord LD, and Martin DS (1993). Potentiation of a three drug chemotherapy regimen by radiation. *Cancer Res* **53**, 3518–3523.

[50] Martin DS, Kligerman MM, and Fugman RA (1958). Radiotherapy and adjuvant combination chemotherapy (6 aminonicotinamide and 6-mertcaptopurine). *Cancer Res* **18**, 893–896.

[51] Varnes ME (1988). Inhibition of pentose cycle of A549 cells by 6-aminonicotinamide: consequences for aerobic and hypoxic radiation response and for radiosensitizer action. *NCI Monogr* 199–203.

[52] Budihardjo, II, Walker DL, Svingen PA, Buckwalter CA, Desnoyers S, Eckdahl S, Shah GM, Poirier GG, Reid JM, Ames MM, and Kaufmann SH (1998). 6-Aminonicotinamide sensitizes human tumor cell lines to cisplatin. *Clin Cancer Res* **4**, 117–130.

[53] Berger NA, Catino DM, and Vietti TJ (1982). Synergistic antileukemic effect of 6-aminonicotinamide and 1,3-bis(2-chloroethyl)-1-nitrosourea on L1210 cells *in vitro* and *in vivo*. *Cancer Res* **42**, 4382–4386.

[54] Keniry MA, Hollander C, and Benz CC (1989). The effect of gossypol and 6-aminonicotinamide on tumor cell metabolism: a ^{31}P magnetic resonance spectroscopic study. *Biochem Biophys Res Commun* **164**, 947–953.

[55] Moyer JD, and Handschumacher RE (1979). Selective inhibition of pyrimidine synthesis and depletion of nucleotide pools by *N*-(phosphonacetyl)-L-aspartate. *Cancer Res* **39**, 3089–3094.

[56] Warnick CT, and Paterson AR (1973). Effect of methylthioinosine on nucleotide concentrations in L5178Y cells. *Cancer Res* **33**, 1711–1715.

[57] Stolfi RL, Stolfi LM, Sawyer RC, and Martin DS (1988). Chemotherapeutic evaluation using clinical criteria in spontaneous, autochthonous murine breast tumors. *J Natl Cancer Inst* **80**, 52–55.

[58] Ben-Horin H, Tassini M, Vivi A, Navon G, and Kaplan O (1995). Mechanism of action of the antineoplastic drug lonidamine: ^{31}P and ^{13}C nuclear magnetic resonance studies. *Cancer Res* **55**, 2814–2821.

[59] Ben-Yoseph O, Lyons JC, Song CW, and Ross BD (1998). Mechanism of action of lonidamine in the 9 L brain tumor model involves inhibition of lactate efflux and intracellular acidification. *J Neurooncol* **36**, 149–157.

[60] Karczmar GS, Arbeit JM, Toy BJ, Speder A, and Weiner MW (1992). Selective depletion of tumor ATP by 2-deoxyglucose and insulin, detected by ^{31}P magnetic resonance spectroscopy. *Cancer Res* **52**, 71–76.

[61] Kaplan O, Jaroszewski JW, Clarke R, Fairchild CR, Schoenlein P, Goldenberg S, Gottesman MM, and Cohen JS (1991). The multidrug resistance phenotype: ^{31}P nuclear magnetic resonance characterization and 2-deoxyglucose toxicity. *Cancer Res* **51**, 1638–1644.

[62] Kaplan O, Navon G, Lyon RC, Faustino PJ, Straka EJ, and Cohen JS (1990). Effects of 2-deoxyglucose on drug-sensitive and drug-resistant human breast cancer cells: toxicity and magnetic resonance spectroscopy studies of metabolism. *Cancer Res* **50**, 544–551.

[63] Rasmussen J, Hansen LL, Friche E, and Jaroszewski JW (1993). ^{31}P and ^{13}C NMR spectroscopic study of wild type and multidrug-resistant Ehrlich ascites tumor cells. *Oncol Res* **5**, 119–126.

[64] Warburg O (1956). On the origin of cancer cells. *Science* **123**, 309–314.

[65] Wike-Hooley JL, Haveman J, and Reinhold HS (1984). The relevance of tumour pH to the treatment of malignant disease. *Radiother Oncol* **2**, 343–366.

[66] Gillies RJ, Liu Z, and Bhujwalla Z (1994). ^{31}P MRS measurements of extracellular pH of tumors using 3-aminopropylphosphonate. *Am J Physiol* **267**, C195–C203.

[67] McCoy CL, Parkins CS, Chaplin DJ, Griffiths JR, Rodrigues LM, and Stubbs M (1995). The effect of blood flow modification on intra- and extracellular pH measured by ^{31}P magnetic resonance spectroscopy in murine tumours. *Br J Cancer* **72**, 905–911.

[68] Roos A (1978). Weak acids, weak bases and intracellular pH. *Respir Physiol* **33**, 27–30.

[69] Raghunand N, Altbach MI, van Sluis R, Baggett B, Taylor CW, Bhujwalla ZM, and Gillies RJ (1999). Plasmalemmal pH-gradients in drug-sensitive and drug-resistant MCF-7 human breast carcinoma xenografts measured by ^{31}P magnetic resonance spectroscopy. *Biochem Pharmacol* **57**, 309–312.

[70] Tannock IF, and Rotin D (1989). Acid pH in tumors and its potential for therapeutic exploitation. *Cancer Res* **49**, 4373–4384.

[71] Raghunand N, Martinez-Zaguilan R, Wright SH, and Gillies RJ (1999). pH and drug resistance: II. Turnover of acidic vesicles and resistance to weakly basic chemotherapeutic drugs. *Biochem Pharmacol* **57**, 1047–1058.

[72] van Bommel EF, Bouvy ND, So KL, Vincent HH, Zietse R, Bruining HA, and Weimar W (1995). High-risk surgical acute renal failure treated by continuous arteriovenous hemodiafiltration: metabolic control and outcome in sixty patients. *Nephron* **70**, 185–192.

[73] Applegate E (1999). Effective nutritional ergogenic aids. *Int J Sport Nutr* **9**, 229–239.

[74] Raghunand N, He X, van Sluis R, Mahoney B, Baggett B, Taylor CW, Paine-Murrieta G, Roe D, Bhujwalla ZM, and Gillies RJ (1999). Enhancement of chemotherapy by manipulation of tumour pH. *Br J Cancer* **80**, 1005–1011.

[75] Rentsch KM, Horber DH, Schwendener RA, Wunderli-Allenspach H, and Hanseler E (1997). Comparative pharmacokinetic and cytotoxic analysis of three different formulations of mitoxantrone in mice. *Br J Cancer* **75**, 986–992.

[76] Moulder JE, and Rockwell S (1987). Tumor hypoxia: its impact on cancer therapy. *Cancer Metastasis Rev* **5**, 313–341.

[77] Thomlinson RH, and Gray LH (1955). The histological structure of some human lung cancers and the possible implications for radiotherapy. *Br J Cancer* **9**, 539–549.

[78] Hockel M, Schlenger K, Mitze M, Schaffer U, and Vaupel P (1996). Hypoxia and radiation response in human tumors. *Semin Radiat Oncol* **6**, 3–9.

[79] Fyles AW, Milosevic M, Wong R, Kavanagh MC, Pintilie M, Sun A, Chapman W, Levin W, Manchul L, Keane TJ, and Hill RP (1998). Oxygenation predicts radiation response and survival in patients with cervix cancer. *Radiother Oncol* **48**, 149–156.

[80] Sotak CH, Hees S HH, Hung MH, Krespan CG, and Raynolds S (1993). A new perfluorocarbon for use in fluorine-19 magnetic

resonance imaging and spectroscopy. *Magn Reson Med* **29** (2), 188–195.

[81] Mason RP, Rodbumrung W, and Antich PP (1996). Hexafluorobenzene: a sensitive ^{19}F NMR indicator of tumor oxygenation. *NMR Biomed* **9**, 125–134.

[82] Swartz HM, and Clarkson RB (1998). The measurement of oxygen *in vivo* using EPR techniques. *Phys Med Biol* **43**, 1957–1975.

[83] Kallman RF (1988). Reoxygenation and repopulation in irradiated tumors. *Front Radiat Ther Oncol* **22**, 30–49.

[84] Hall EJ (1988). In *Radiobiology for the Radiologist*. J.B. Lippincott, Philadelphia, PA. p. 154.

[85] O'Hara J, Goda F, Demidenko E, and Swartz HM (1998). Effect on regrowth delay in a murine tumor of scheduling split-dose irradiation based on direct pO_2 measurements by electron paramagnetic resonance oximetry. *Radiat Res* **150**, 549–556.

[86] Smirnov AI, Norby SW, Clarkson RB, Walczak T, and Swartz HM (1993). Simultaneous multi-site EPR spectroscopy *in vivo*. *Magn Reson Med* **30**, 213–220.

[87] Swartz HM, and Halpern H (1998). EPR Studies of Living Animals and Related Model Systems (*In Vivo* EPR). In *Spin Labeling: The Next Millenium*. LJ Berliner (Ed). Plenum Publishing, New York, NY. pp. 367–404.

[88] Robinson SP, Howe FA, and Griffiths JR (1995). Non-invasive monitoring of carbogen-induced changes in tumor blood flow and oxygenation by functional magnetic resonance imaging. *Int J Radiat Oncol Biol Phys* **33**, 855–859.

[89] Karczmar GS, River JN, Li J, Vijayakumar S, Goldman Z, and Lewis MZ (1994). Effects of hyperoxia on T_2^* and resonance frequency-weighted magnetic resonance images of rodent tumours. *NMR Biomed* **7**, 3–11.

[90] Griffiths JR, Taylor NJ, Howe FA, Saunders MI, Robinson SP, Hoskin PJ, Powell ME, Thoumine M, Caine LA, and Baddeley H (1997). The response of human tumors to carbogen breathing, monitored by gradient-recalled echo magnetic resonance imaging. *Int J Radiat Oncol Biol Phys* **39**, 697–701.

[91] Al-Hallaq HA, Zamora M, River JN, and Karczmar GS (1999). MR Correctly Predicts the Relative Effect of Two Tumor-Oxygenating Agents on Hypoxic Fraction in Rodent BA1112 Tumors. In *ISMRM 7th Scientific Meeting*. ISMRM, Philadelphia, Pennsylvania, USA.

[92] Al-Hallaq HA, River JN, Zamora M, Oikawa H, and Karczmar GS (1998). Correlation of magnetic resonance and oxygen microelectrode measurements of carbogen-induced changes in tumor oxygenation. *Int J Radiat Oncol Biol Phys* **41**, 151–159.

[93] Dunn JF, and Swartz HM (1997). Blood oxygenation. Heterogeneity of hypoxic tissues monitored using bold MR imaging. *Adv Exp Med Biol* **428**, 645–650.

[94] Vexler VS, de Crespigny AJ, Wendland MF, Kuwatsuru R, Muhler A, Brasch RC, and Moseley ME (1993). MR imaging of blood oxygenation-dependent changes in focal renal ischemia and transplanted liver tumor in rat. *J Magn Reson Imaging* **3**, 483–490.

[95] Moolten FL (1986). Tumor chemosensitivity conferred by inserted herpes thymidine kinase genes: paradigm for a prospective cancer control strategy. *Cancer Res* **46**, 5276–5281.

[96] Hamstra DA, Rice DJ, Fahmy S, Ross BD, and Rehemtulla A (1999). Enzyme/prodrug therapy for head and neck cancer using a catalytically superior cytosine deaminase. *Hum Gene Ther* **10**, 1993–2003.

[97] Gambhir SS, Herschman HR, Cherry SR, Barrio JR, Satyamurthy S, Toyokuni T, Phelps ME, Larson SM, Balatoni J, Finn R, Tjuvajev J, and Blasberg R (2000). Imaging transgene expression with radionuclide imaging technologies. *Neoplasia* **2**, 118–138.

[98] Stegman LD, Rehemtulla A, Beattie B, Kievit E, Lawrence TS, Blasberg RG, Tjuvajev JG, and Ross BD (1999). Noninvasive quantitation of cytosine deaminase transgene expression in human tumor xenografts with *in vivo* magnetic resonance spectroscopy. *Proc Natl Acad Sci USA* **96**, 9821–9826.

[99] Rainov NG, Zimmer C, Chase M, Kramm CM, Chiocca EA, Weissleder R, and Breakefield XO (1995). Selective uptake of viral and monocrystalline particles delivered intra-arterially to experimental brain neoplasms. *Hum Gene Ther* **6**, 1543–1552.

[100] Weissleder R, Simonova M, Bogdanova A, Bredow S, Enochs WS, and Bogdanov A, Jr. (1997). MR imaging and scintigraphy of gene expression through melanin induction. *Radiology* **204**, 425–429.

[101] Moore A, Basilion JP, Chiocca EA, and Weissleder R (1998). Measuring transferrin receptor gene expression by NMR imaging. *Biochim Biophys Acta* **1402**, 239–249.

[102] Izquierdo M, Cortes M, de Felipe P, Martin V, Diez-Guerra J, Talavera A, and Perez-Higueras A (1995). Long-term rat survival after malignant brain tumor regression by retroviral gene therapy. *Gene Ther* **2**, 66–69.

[103] Ross BD, Kim B, and Davidson BL (1995). Assessment of ganciclovir toxicity to experimental intracranial gliomas following recombinant adenoviral-mediated transfer of the herpes simplex virus thymidine kinase gene by magnetic resonance imaging and proton magnetic resonance spectroscopy. *Clin Cancer Res* **1**, 651–657.

[104] Beer SJ, Matthews CB, Stein CS, Ross BD, Hilfinger JM, and Davidson BL (1998). Poly (lactic–glycolic) acid copolymer encapsulation of recombinant adenovirus reduces immunogenicity *in vivo*. *Gene Ther* **5**, 740–746.

[105] Hamstra DA, Rice DJ, Pu A, Oyedijo D, Ross BD, and Rehemtulla A (1999). Combined radiotherapy and enzyme/prodrug therapy for head and neck cancer in an orthotopic animal model. *Radiat Res* **152**, 499–507.

[106] Namba H, Tagawa M, Iwadate Y, Kimura M, Sueyoshi K, and Sakiyama S (1998). Bystander effect-mediated therapy of experimental brain tumor by genetically engineered tumor cells. *Hum Gene Ther* **9**, 5–11.

[107] Nordsmark M, Maxwell RJ, Wood PJ, Stratford IJ, Adams GE, Overgaard J, and Horsman MR (1996). Effect of hydralazine in spontaneous tumours assessed by oxygen electrodes and ^{31}P magnetic resonance spectroscopy. *Br J Cancer Suppl* **27**, S232–235.

[108] Shine N, Palladino MA, Jr., Patton JS, Deisseroth A, Karczmar GS, Matson GB, and Weiner MW (1989). Early metabolic response to tumor necrosis factor in mouse sarcoma: a phosphorus-31 nuclear magnetic resonance study. *Cancer Res* **49**, 2123–2127.

[109] Constantinidis I, Braunschweiger PG, Wehrle JP, Kumar N, Johnson CS, Furmanski P, and Glickson JD (1989). ^{31}P nuclear magnetic resonance studies of the effect of recombinant human interleukin 1 a on the bioenergetics of RIF-1 tumors. *Cancer Res* **49**, 6379–6382.

[110] Evelhoch JL, Bissery MC, Chabot GG, Simpson NE, McCoy CL, Heilbrun LK, and Corbett TH (1988). Flavone acetic acid (NSC 347512)-induced modulation of murine tumor physiology monitored by *in vivo* nuclear magnetic resonance spectroscopy. *Cancer Res* **48**, 4749–4755.

[111] Breidahl T, Nielsen FU, Maxwell RJ, Stødkilde-Jørgensen H, and Horsman MR (1999). Evaluating The Anti-Tumour Activity of New Vascular-Damaging Agents Using Magnetic Resonance Spectroscopy. In *ISMRM 7th Scientific Meeting*. ISMRM, Philadelphia, PA.

[112] Galbraith SM, Taylor NJ, Stirling JJ, Rustin G, and Baddeley H (1999). Dynamic Contrast-Enhanced MRI to Monitor Perfusion and Permeability Changes in Human Tumours During Treatment by the Vascular Targeting Agent DMXAA. In *ISMRM 7th Scientific Meeting*. ISMRM, PA, Philadelphia.

[113] Beauregard DA, Thelwall PE, Chaplin DJ, Hill SA, Adams GE, and Brindle KM (1998). Magnetic resonance imaging and spectroscopy of combretastatin A4 prodrug-induced disruption of tumour perfusion and energetic status. *Br J Cancer* **77**, 1761–1767.

[114] Maxwell RJ, Nielsen FU, Breidahl T, Stodkilde-Jorgensen H, and Horsman MR (1998). Effects of combretastatin on murine tumours monitored by ^{31}P MRS, ^{1}H MRS and ^{1}H MRI. *Int J Radiat Oncol Biol Phys* **42**, 891–894.

[115] Abramovitch R, Frenkiel D, and Neeman M (1998). Analysis of subcutaneous angiogenesis by gradient echo magnetic resonance imaging. *Magn Reson Med* **39**, 813–824.

[116] Sipkins DA, Cheresh DA, Kazemi MR, Nevin LM, Bednarski MD, and Li KC (1998). Detection of tumor angiogenesis *in vivo* by $\alpha_v\beta_3$-targeted magnetic resonance imaging. *Nat Med* **4**, 623–626.